Uniaxial compression of fibre networks – the synergetic effect of adhesion and elastoplasticity on non-reversible deformation

(article starts on next page)

Uniaxial compression of fibre networks – the synergetic effect of adhesion and elastoplasticity on non-reversible deformation

Per Bergström [a,b,*], Charlotta Hanson [b,c], Henrik Ström [a], Srdjan Sasic [a]

[a] Department of Mechanics and Maritime Sciences – Division of Fluid Dynamics, Chalmers University of Technology, Gothenburg, Sweden
[b] Essity Hygiene and Health AB, Mölndal, Sweden
[c] Department of Chemistry and Chemical Engineering, Chalmers University of Technology, Gothenburg, Sweden

ARTICLE INFO

ABSTRACT

In this paper we study numerically and experimentally non-reversible deformation of anisotropic, semi-flexible fibre networks. We formulate a Discrete Element Model (DEM) with bonded particles to simulate uniaxial compression of such networks and use this model to describe and quantify the effect of elasto-plastic fibre contacts and fibre-fibre adhesion on non-reversible deformation. Our results show that inter-fibre adhesion plays a role for compression in a low solid volume fraction range where adhesive forces can overcome fibre deformation forces and moments. Also, elasto-plastic contacts between fibres become important at higher solid volume fractions when the yield criterion is exceeded. The combined case of fibres having elasto-plastic contacts and adhesion shows a significant synergetic effect leading to a degree of non-reversible deformation of the network far beyond that of networks with only elasto-plastic fibre contacts or inter-fibre adhesion.

1. Introduction

A fibre network is a ubiquitous structure commonly seen in man-made materials (paper, hygiene products and nonwoven), biological materials (collagen fibre networks and cytoskeleton of eukaryotic cells), and polymers (rubber and hydrogels). A number of subclasses exist for fibre networks, such as bonded (cross-linked) vs. non-bonded (entangled) ones, flexible vs. semi-flexible, and anisotropic vs isotropic fibre networks [1]. In bonded fibre networks inter-fibre bonds restrict *fibre rearrangement*, understood as the relative sliding of fibres during network deformation, leading to more mechanically stable structures, while non-bonded fibre networks are more prone to non-reversible deformation from tensile or compressive strain. Fibre networks are often used for their mechanical properties in relation to weight, as well as their fluid transport properties due to the inherent permeable nature of these materials. The packing density of the fibres in the network is often characterized by the bulk density, or as we choose in this paper, the closely related *solid volume fraction* defined as the ratio of solid material volume to total volume. These characteristics have a strong influence on mechanical and fluid transport properties of the networks. This influence is often used in both nature and

industry to tailor materials with specific properties such as in the nonwoven, paper tissue and absorbent product industries, where controlling of inter-fibre bonding and the degree of compaction is used to design materials with specific properties in terms of tensile strength, softness and permeability. In these cases, compaction of the network is often done in the form of compression by applying uniaxial pressure in the production process to induce non-reversible deformation of the network in order to achieve the desired solid volume fraction and, in consequence, the desired mechanical and fluid transport properties of the network. Compaction and controlling the solid volume fraction of fibre networks are hence key parts of several industrial processes.

The studying of compression of fibre networks goes back to the textile industry in the mid-20th century where van Wyk developed a semi-empirical model for pressure as a function of solid volume fraction [2]. The work was followed by further development of statistical models by, for example, Komori [3] and Toll [4]. However, these models relied on some simplifying assumptions, such as affine deformation of fibre-fibre contacts, which did not account for fibre rearrangement in the form of sliding and led to fully reversible deformation during loading-unloading.

More recent work includes numerical studies of non-bonded fibre networks primarily using discrete element (DEM) or bead-spring models to capture fibre deformation and also to account for fibre-fibre rearrangement. The latter is an important aspect especially in non-bonded networks as it significantly impacts both the overall response and the non-reversible deformation of these soft materials. Important

* Corresponding author at: Department of Mechanics and Maritime Sciences – Division of Fluid Dynamics, Chalmers University of Technology, Gothenburg, Sweden.
E-mail address: per.bergstrom@chalmers.se (P. Bergström).

findings from the studies include the relationship between density and network pressure during compression. A study by Barbier et al. confirmed that stresses followed the predicted dependence on density by van Wyk, a power function with an exponent of 3, and that the number of fibre-fibre contacts increased linearly with density [5]. Ban et al. found that for networks consisting of fibres with varying fibre stiffness, the overall network stiffness decreased as the variability of the fibre stiffness increased at a constant mean fibre stiffness [6].

Other significant findings relate to the characteristic transitions of deformation mode that occur during compression of fibre networks. Rodney et al. studied the packing density and entanglement transition of such networks and found that the entanglement transition which happens when mechanical equilibrium is achieved under non-zero applied pressure occurs at a much smaller volume fraction for longer fibres than for shorter ones [7]. Subramanian and Picu studied triaxial compression of semiflexible fibre networks and found that in a low density regime of compression the fibre strain energy is associated primarily with the bending of fibres, while at higher densities it transitions to being stored primarily in the axial deformation mode [8]. Hossain et al. looked at uniaxial compression, as opposed to triaxial, and found that the fibre strain energy is associated primarily with the bending of fibres at lower densities, while at higher densities it transitions to primarily being stored in the transverse contact deformation mode as opposed to the axial deformation mode [9]. When studying the role of friction in compression of fibre networks, Barbier et al. found that friction between fibres led to increased energy stored in the fibre axial deformation mode and increased network pressure during loading, while axial deformation energy reducing sharply during unloading led to a more pronounced hysteresis in the loading-unloading cycle [5]. Guo et al. studied macroscopic response to uniaxial compression of flexible fibre networks with varying fibre aspect ratios (2–25). It was found that the response could be divided into the following three regimes: yielding, transitional and hardening. High fibre aspect ratios, friction and confining pressure were found to promote a hardening behaviour [10]. The transition behaviour of semi-flexible fibre networks is also known in tensile deformation of bonded fibre networks, from the work by Head et al., where the fibre deformation mode transitions between bending and axial deformation depending on network density and deformation [11].

Overall, these findings paint the picture of semi-flexible fibre networks as being a class of materials with a wide range of regimes and with very varying responses to stress. The regime that prevails is dependent on the network properties such as density, and fibre properties such as aspect ratio and fibre stiffness in the different deformation modes, as well as on the form of network compression.

Given the strong and nonlinear dependence of compressive stiffness, tensile strength and also other network properties such as fluid permeability on the network density, non-reversible deformation of networks due to compression becomes significant in understanding the behaviour of this type of materials. At the same time, due to the soft and deformable nature of such networks, large non-reversible deformation is commonly seen experimentally, e.g. [12], showing compression of an originally low density network leading to a solid volume fraction of greater than 0.2 after unloading. Non-reversible deformation is also commonly used in industrial applications when designing networks with various desired properties [13]. We also note that the presence of moisture or humidity is known to significantly influence the mechanics of nonbonded fibre networks and that pulp fibres, even in a "dry" state, still contain a considerable amount of liquid at room temperature and 50% relative humidity, typically around 5–10 wt%. This presence of moisture and the dependence of network mechanics on humidity suggests the existence of effects of inter-fibre adhesion or elasto-plastic deformation of fibres on non-reversible deformation. Despite these implications, not much modelling work has been done in the research community in characterizing and studying the phenomena behind non-reversible compressive deformation in non-bonded semi-flexible

fibre networks. Some studies did, however, observe non-reversible deformation in simulations. Subramanian and Picu observed a small difference between first and subsequent loadings in triaxial compression of semiflexible fibre networks using a bead-spring model, which was attributed to fibre rearrangement [8]. Barbier et al. performed modelling of triaxial compression of semi-flexible fibre networks to study the effect of friction on hysteresis during loading-unloading cycles. Non-reversible strain was observed between first and second loadings and the authors chose to study only subsequent loadings in order not to account for this strain [5]. Guo et al. modelled uniaxial compression of low aspect-ratio rubber cords. Loading stress during a second load-cycle was observed to be reduced both in experiments and simulations and attributed to compaction from the first load-cycle [14]. These studies, however, involved networks of elastic fibres without inter-fibre adhesion or plastic deformation, which led to the fact that the only effects that contributed to non-reversible deformation of the network were fibre rearrangement due to sliding and fibre deformation due to fibre-fibre friction. As a consequence, in such studies non-reversible deformation was observed on a level that is considerably less than that commonly seen in industrial applications. This fact raises the question of the origin of large non-reversible deformation in this type of networks and the possible impact of adhesion and plastic deformation of fibres due to their known dependence on moisture and humidity. In this work we will characterize and explain these effects.

The effect of inter-fibre adhesion on the mechanics of fibre networks has been studied and shown to have significant impact on the response of networks. Picu and Sengab characterized adhesion-driven structural evolution and fibre bundling of nonbonded fibre networks [15]. Guo et al. used DEM to simulate the dynamics of wet, semi-flexible fibres [16]. Negi and Picu studied response of planar fibre networks stabilised by fibre-fibre adhesion due tensile loading [17]. The same authors studied mechanical behaviour of bonded fibre networks with inter-fibre adhesion in uniaxial tension and compression using a 2D model [18]. The results in compression for small strains showed an initial linear elastic regime followed by strain localization.

Elasto-plastic deformation of fibres can occur either in the form of plastic contact deformation in the fibre-fibre contact points or in the form of plastic bending deformation due to large moments exerted on the fibre. The effect of these forms of plastic deformation has been addressed previously and shown to result in the existence of a significant impact on mechanical response from compression. Guo et al. developed a bonded sphero-cylinder model to simulate fibres that undergo plastic bending deformation and validated the results for single fibres using a finite element model [19]. Leblicq et al. used DEM to model crop stems where the effect of plastic contact deformation was incorporated in the model, and non-reversible deformation of the network was observed in uniaxial compression of a small number of fibres [20]. Guo et al. simulated uniaxial compression of fibre assemblies by studying compression force development and hysteresis in the loading-unloading cycle for different contact force models and plastic deformation of fibres. Elastic fibres were compared to elasto-plastic ones experiencing plastic deformation due to both bending and contact deformation. It was found that the elastic fibre bending model significantly overpredicted the loads in the low solid volume fraction range where bending dominated and that the elastic fibre-fibre contact model overpredicted the loads in the high solid volume fraction range where contact deformation was dominant [21].

In this study we examine non-reversible deformation due to large network strain from uniaxial compression in non-bonded, semi-flexible, anisotropic networks. Such networks are commonly seen in papers, hygiene products, nonwovens and also some biological fibre networks. The effect of non-reversible deformation on network solid volume fraction is crucial in understanding this class of materials in terms of mechanical response, as well as fluid transport and other properties. In particular, we note that large non-reversible deformation is commonly seen in these types of materials, something which has not

been captured in previous modelling work. In this work we specifically look at compression of a pulp fibre network commonly found in baby diapers, feminine pads and incontinence pads. The networks are created by air-laid fibres creating a low-density anisotropic network known to be very soft and prone to non-reversible deformation. We therefore model fibre networks in 3D using DEM to represent non-bonded fibres with stiffnesses in normal, shear, bend and twist that interact with friction, inter-fibre adhesion and elasto-plastic fibre-fibre contact deformation. We have chosen not to incorporate plastic deformation due to bending in our model. We base this choice on findings from the literature that fibre shape was unaffected after the pulp fibre network had been subjected to high compression pressures and large degrees of non-reversible deformation [22]. The numerical framework is used to characterize the effect of adhesion and plastic contact deformation of fibres on the non-reversible deformation of the network to further understand the nature of this class of materials. The approach used here is to model different cases of fibre-fibre contact mechanics separately in order to isolate the various phenomena of contact mechanics and compare the characteristics of the obtained response to the measurements. Such an approach results in four different cases of contact mechanics evaluated. First, we have the case with elastic fibres without adhesion, and then look at elastic fibres with adhesion. After that, we study the effect of elasto-plastic contacts between fibres without adhesion and, finally, we investigate the combined effect of elasto-plastic contacts between fibres and adhesion.

2. Measurements

We performed measurements to look at characteristic behaviour of fibre networks during uniaxial compression. The network tested consisted of air laid Southern Pine pulp fibres with an areal density of 400 g/m^2, a type of fibre network often found in hygiene products such as diapers, incontinence pads and feminine pads. The process of creating the network involves separated fibres transported in air being deposited on a perforated plate resulting in a low-density anisotropic network. Fibres had an average length of 1.8 mm with coarseness 0.27 mg/m, curl index of 0.14 and effective fibre density of 1000 kg/m^3.

The tests were performed at 23°C and RH 50% using an Instron tester equipped for compression measurements. The sample network was placed on a flat base and compressed at slow speed using a flat probe with a circular cross section of 11 mm diameter and with the size of the sample being larger than the diameter of the probe. Each test consisted of two sequences of loading-unloading in the same spot to characterize the development of pressure vs. solid volume fraction for two repeated loadings. Two cases of measurements were performed where different samples were compressed up to 10 kPa and 1000 kPa, respectively.

The pressure response from the network when increasing the solid volume fraction, SVF, by means of compression, is shown in Fig. 1. The difference between the first and second loading is due to the non-reversible deformation caused by the first loading. We see in both cases, compression to 10 kPa and to 1000 kPa, that the pressure response is lower at a given solid volume fraction in the second compression compared to the first one for the entire range of SVF tested up to the point of maximum pressure tested. At this point the curves from the first and second loading collapse.

We use the term *initial solid volume fraction* to describe the solid volume fraction when the compression is starting to affect the fibre network, not only touching or compressing single fibres sticking out of the sample. The pressure at which the initial solid volume fraction is defined is 0.1 kPa in accordance with the procedure from [23]. The initial solid volume fraction can serve as a measure for the comparison of different compression schemes. A difference in the initial solid volume fraction between the first and second compression is the measure we use to establish whether the non-reversible deformation i.e., permanent compression of the network was obtained.
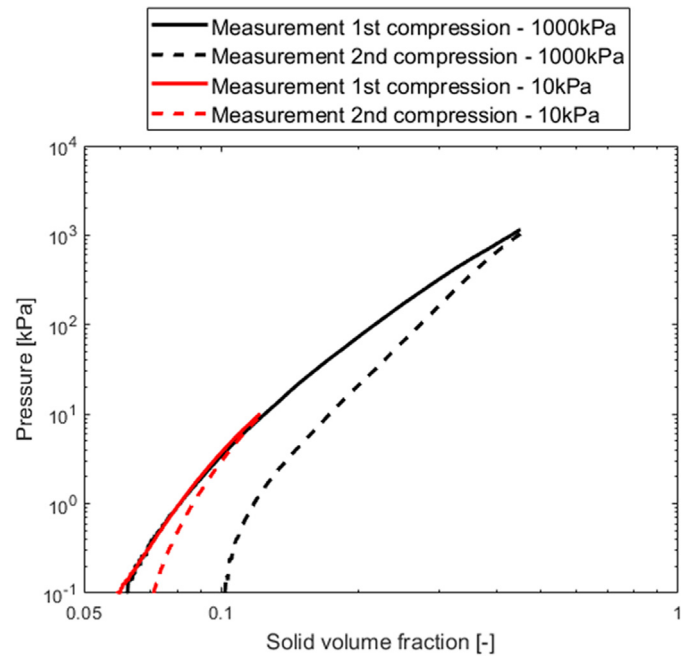

Fig. 1. Pressure vs. solid volume fraction measured for two samples of pulp fibre networks. Each measurement consists of a sequence of two repeated compression–unloading cycles with the second compression intended to characterize the network deformation sustained from the first compression. The two different measurements are labelled 1000 kPa and 10 kPa based on the maximum pressure applied during compression.

In the measured samples the initial solid volume fraction was 0.06 at the first compression. After compressing up to 10 kPa, the initial solid volume fraction before the second compression had increased to 0.07 (Fig. 1), while compression up to 1000 kPa increased the initial solid volume fraction more, to 0.10.

In summary, the measurements show a significant impact on non-reversible deformation from the first compression through the entire pressure range tested, both for the tests with low and high maximum compressive forces.

3. Methodology

3.1. Discrete element modelling

In this work, fibre networks are modelled on a single fibre level using Discrete Element Modelling (DEM). Particle interactions can take various forms, such as contact interactions in the normal direction, for example compressibility of particles, and tangential direction through inter-particle friction. Particles may also be bonded together and interacting through forces or torques between the bonded particles. The law governing this system of particles is the conservation of linear momentum and angular momentum:

$$m_i \ddot{\boldsymbol{r}}_i = \sum_j \boldsymbol{F}_{ij} + \boldsymbol{F}_i^b, \tag{1}$$

$$\frac{\partial}{\partial t}(\boldsymbol{I}_i \cdot \boldsymbol{\omega}_i) = \sum_j \boldsymbol{T}_{ij}, \tag{2}$$

where m_i is the mass and $\boldsymbol{r}_i$ is the position vector of the i-th particle, $\boldsymbol{F}_{ij}$ is the interaction force between the i-th and j-th particles and $\boldsymbol{F}_i^b$ is the body force acting on the i-th particle. For angular momentum, $\boldsymbol{I}_i$ is the moment of inertia tensor, $\boldsymbol{\omega}_i$ is the angular velocity and $\boldsymbol{T}_{ij}$ is the interaction torque between the i-th and j-th particles. In this work fibres are modelled as a string of connected spherical particles as illustrated in Fig. 2, linked by bonds with stiffnesses in the normal, shear, twist and

Fig. 2. Illustration of a fibre modelled as a string of 110 connected particles.

Fig. 3. The relationship between adhesive force and surface to surface separation.

bend modes, while non-bonded particles can interact by normal and tangential contact forces. For bonded particles the contact interaction is disabled and the interaction forces, F_{ij}, and moments, T_{ij}, come from the bonded interaction. The choice of spherical particles as opposed to spherocylindrical or other particle shapes was based on improved time for contact search and longer time steps allowed without introducing erroneous rotational kinetic energy. In relation to the latter choice, the reader is further referred to [19]. In this work we are using the open source DEM software LIGGGHTS [24] with particle-particle bonds based on the work by Richter [25] and Schramm et al. [26]. This results in a representation of fibres that facilitates translation, rotation and relative sliding of fibres, while at the same time capturing fibre geometry, mechanical properties and contact interactions of fibres.

3.2. Contact force models

Contacts between non-bonded particles are modelled as elastic or elasto-plastic, and with or without taking into account the adhesive force between particles. An elastic contact is modelled using a Hertzian contact model with Coulomb friction using an elastic modulus for contact of 1 GPa [27] and friction coefficient of 0.3.

Elasto-plastic contacts between fibres are modelled based on the contact model by Thornton and Ning [28], as implemented by Loh et al. [29]. The implementation is based on tabulation-scaling implementation that closely approximates the elastic–adhesive unloading curve for a particle contact as modelled by Thornton and Ning. In this model, the contact can become plastic if the contact radius exceeds the one at which yield occurs, a_y, here forth expressed in terms of yield ratio $c_y = a_y/D$. In this model, the particle-particle unloading force depends on the deformation history of the contact. If the contact is in a plastic state just before unloading, then the contact stiffness becomes dependent on the amount of previous plastic deformation and a new effective radius of the particle is calculated and stored.

Adhesion between fibres in DEM has been represented in a number of ways in literature. A recent example is by e.g. Guo et al. [16] who used the liquid bridge force model by Mikami et al. [30]. For pulp fibre networks adhesion between fibres can have contributions from several different origins, e.g. van der Waals forces, Coulomb forces, capillary forces, mechanical interlocking, etc. In order to reflect the adhesive force between pulp fibres in air-dry state we use measurements by Andersson [31] to choose an adhesive force maximum of F_{adh} of 25 μN. The separation distance was chosen to be 1 μm based on it being a relevant separation distance for both capillary forces and mechanical interlocking, as well as computationally viable since smaller separation distances would require decreased time step sizes and increased computational costs. We choose in this work to implement the adhesion between fibres based on the model for capillary forces with fixed liquid bridge by Rabinovich et al. [32] [33] and to calibrate the model to reflect the given maximum adhesive force and separation distance.
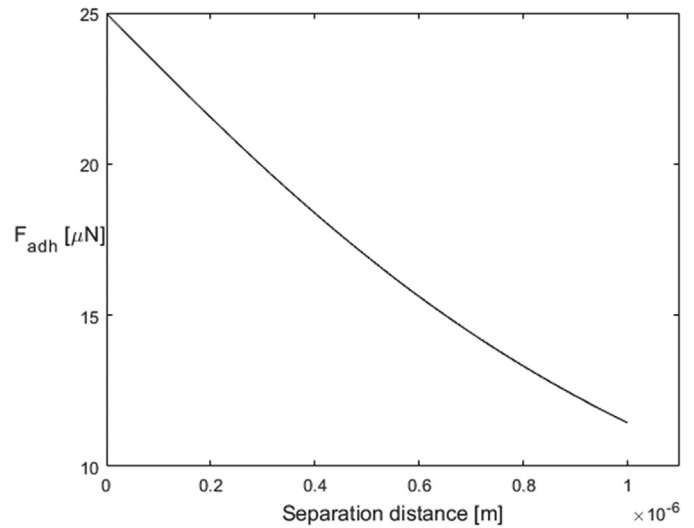
The resulting adhesive force as a function of surface-to-surface separation distance can be seen in [Fig. 3].

3.3. Fibre properties

The networks tested consist of 3000 fibres with a fibre length of $\lambda = 2$ mm, each fibre consisting of 110 particles of diameter $D=18\mu m$ [Fig. 4]. Fibres have a coarseness (fibre mass per unit length) of 0.27 mg/m, which corresponds to an effective fibre density of 1000 kg/m3, and a curl index $((Le-\lambda)/\lambda)$ of 0.15, where Le is the end-to-end distance of fibres. The cross section of the modelled fibres is inherently circular due to the spherical particles used as opposed to the more elliptical or rectangular cross section of the pulp fibres. The chosen diameter of the particles is based on matching the cross-sectional area of the simulated fibre with the measured fibre. The rationale here is to match the fibre volume and in consequence match the solid volume fraction of the simulated and the measured networks based on the well-known dependence of pressure and fibre-fibre contacts on solid volume fraction [2,4]. The bonded particles are spaced one diameter apart leading to a slight surface roughness of the fibre as seen in [Fig. 2]. The effect of the surface roughness of fibres due to the connected particle representation has been studied by Picu and Subramanian [8,34] who found that roughness had not led to artificial friction or adhesion of fibres in contact.

Stiffness of the fibres is defined in bending, axial, shear and twist modes as $k_b = E_f I/D$, $k_a = E_f A/D$, $k_s = G_f A/D$ and $k_t = G_f J/D$, respectively. Young's modulus of the fibres is $E_f = 4GPa$ based on the bending stiffness over the long axis of the fibre cross section from the work by Lorbach et al. [35].

3.4. Network generation

Network configuration and properties like fibre orientation and connectivity play an important role in the network response to compression. To create a realistic initial network for use in the simulations, fibres are generated randomly in a dilute suspension, deposited by gravity and consolidated to form a mechanically stable low-density anisotropic fibre network with similar characteristics to what is commonly seen in papers, hygiene products and nonwovens. The centre points of the generated fibres being $0 < x < 0.01$ m, $0 < y < 0.01$ m and $0 < z < 0.07$ m were used to generate a 1×1 cm deposited network with an initial solid volume fraction of 0.06, matching the networks from measurements in Section 2. In terms of the resulting generated

Fig. 4. Illustration of fibre network used in the simulations. The network consists of 3000 fibres with a length of 2 mm deposited in a 1x1cm area.

structures this method is distinct from other methods of network generation, such as directly generating the final network configuration, single fibre deposition, or the method of placing seed points and then growing individual fibres in 3D, in producing a mechanically stable and inherently anisotropic network.

3.5. Mechanical testing

Uniaxial compression of the generated network is performed by having a virtual wall compress the network from above. There are no constraints in the x and y-directions and pressure measured in the interior area of the sample to exclude edge effects from decreasing areal density close to the edges of the sample. The compressing wall is moved in sequences of slow compression followed by a relaxation time, to allow kinetic energy to dissipate, after which pressure values are measured. Containing the kinetic energy while also avoiding artificial pressure from damping in the system is a major challenge in modelling our system, especially for low pressure measurements. During the unloading phase, the excess kinetic energy can lead to oscillations and excessive breakage of adhesive bonds in the network. The issue can be seen by, for example, monitoring the number of fibre-fibre contacts for the network where the excess kinetic energy leads to oscillations in the number of contacts, or by monitoring individual contacts where the issue can be seen as particles alternating between being in and not in contact. In order to achieve quasi-static measurements of pressure and to avoid erroneous effects from the kinetic energy created in the sample, we monitor the kinetic energy in relation to the fibre deformation energy as suggested by Abd El-Rahman and Tucker [36]. We take steps to reduce the kinetic energy, such as prescribing low velocity of the compressing wall, ramping up/down wall velocity when starting and stopping, long waiting time during relaxation and a low time-step size. All these measures combined lead to simulations with considerable computational times.

To characterize the network during the compression-unloading sequence we calculate the fibre deformation energy and number of fibre-fibre contacts. The fibre deformation energy, E_{def}, is calculated for each intra-fibre bond as the sum of the deformation energy in each of the four modes: bending, axial, shear and twist.

$$E_{def} = \frac{k_b}{2}\theta_b^2 + \frac{k_a}{2}\delta_a^2 + \frac{k_s}{2}\delta_s^2 + \frac{k_t}{2}\theta_t^2,$$ (6)

where θ and δ are displacements from equilibrium angles and distances, respectively, and k is the corresponding stiffness. The fibre-fibre contacts are counted as individual contacts between two fibres which can

consist of more than one particle-particle pair between consecutive particles of two fibres.

4. Results and discussion

4.1. Network properties if only elastic contacts assumed

We begin by using an elastic contact model to study compression and non-reversible deformation in a fibre network. [Fig. 5] shows pressure vs. solid volume fraction (SVF) of the simulated network compared to the measurements described in Section 2 for two consecutive compressions. Here, the second loading is used to characterize the non-reversible deformation caused by the first loading.

Comparing the loading curves of the first compressions [Fig. 5], we see that the curve for the simulated pressure follows the measurement well for very low pressure and continues to follow the overall trend of the pressure development seen in the measurements, while overestimating the pressure up to around one order of magnitude at the point of maximum compression.

When looking at the second loading, we see that for the simulated network the pressure starts at the same SVF as for the first loading and that the pressure curves for the two loadings follow each other very closely. This behaviour differs from the measured characteristics, where the second loading starts having pressure at a significantly higher SVF than for the first loading. Also, the pressure for the second compression is reduced compared to the first loading for the entire range of SVF up to the point of maximum compression. This finding clearly indicates that there has been no non-reversible deformation caused by the first loading in the simulated results. We corroborate this conclusion by looking at the number of fibre-fibre contacts in the network. The number of fibre-fibre contacts per fibre has for long been known to correlate with the network SVF [3,4], and used as a way of characterizing network density. We therefore study the development of the number of fibre-fibre contacts during compression and unloading, focusing on their number that remains during the unloading of the network. An increased number of fibre-fibre contacts after the compression-unloading-cycle compared to their number before compression would indicate a change in network configuration, and in consequence the network properties, due to deformation of the network.

When looking at the development of fibre-fibre contacts [Fig. 6] we see an extremely close correlation to the predicted values from the statistical model by Toll [4]. Comparing the simulated curves for loading and unloading, we see that the number of contacts during unloading retraces the path from the loading curve very closely, returning to the
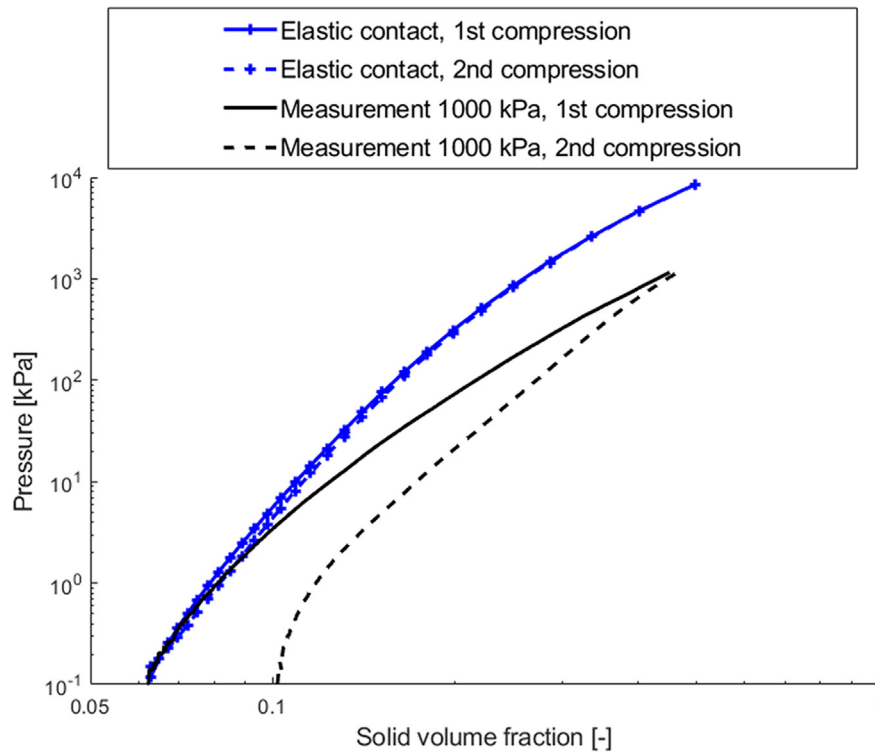
Fig. 5. Simulation vs. measurements of the first and second compression. The simulated network involves only elastic contacts. The simulated results show that for the chosen network the pressure development for the second loading overlaps with that of the first loading. This indicates that there has been no non-reversible deformation caused by the first loading in the simulated results.
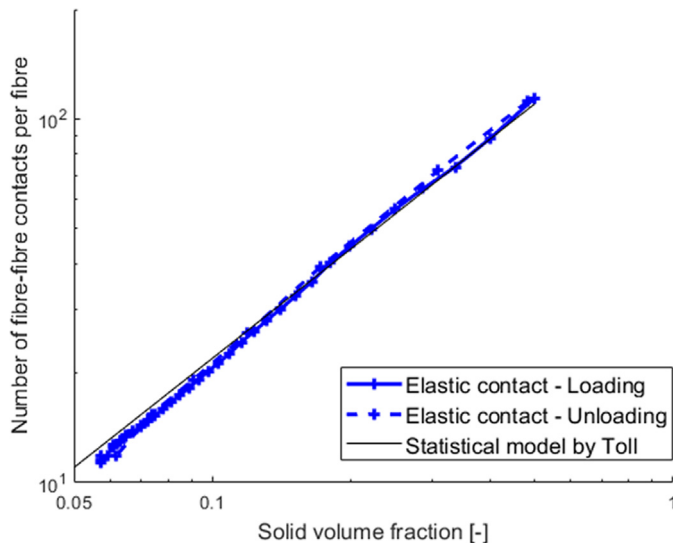

Fig. 6. Number of fibre-fibre contacts per fibre for the simulated network with elastic contacts during loading (solid blue) and unloading (dashed blue). A statistical model by Toll (black) is presented as a reference. The results show the number of fibre-fibre contacts during unloading overlapping with the loading curve and returning to the original number of fibre-fibre contacts after unloading.

same number of fibre-fibre contacts after unloading as before compression. This again indicates that the network has returned to the original configuration without sustaining any non-reversible deformation.

We conclude that our use of elastic fibres given the simulated fibre and network properties fails to reproduce non-reversible deformation due to compression. Also, the simulated compressive pressure for the repeated loading is not corresponding well with the measurements. This is not surprising, and a direct result of the chosen setup not

capturing the deformation of the network from the first compression. All in all, these conclusions signify the impact of the physics not accounted for in the simulations when the fibres are having elastic contacts only.

4.2. Network properties for elastic contacts with adhesion

We continue by looking at compression of the same fibre network as in the previous section, but we now add inter-fibre adhesion. The goal is to characterize the role that inter-fibre adhesion plays in non-reversible deformation of the network from a first compression, and to also see how pressure develops during a second loading. For the simulations we choose the maximum adhesive force between fibres to be 25 μN based on the measurements by Andersson [31]. We will compare the obtained results to the case where no adhesive forces are present. In addition, we will look at the effect of using an exaggerated effect of adhesion by a factor of ten, using the maximum fibre adhesive force of $250\mu N$.

From the results for the first compression of the network we can see [Fig. 7] that an increase in the inter-fibre adhesion force creates a slight increase in pressure in the very low pressure range, while at the later stages of compression the curves collapse. We argue that adhesion has an effect on pressure in a low SVF network, where fibres are less entangled and can move more freely in relation to each other. In later stages of compression, the effect of adhesion is marginalized.

Looking at the second compression of the network [Fig. 8], we see some effect of the inter-fibre adhesion on non-reversible deformation of the network from the first compression. The *initial solid volume fraction*, measured at 0.1 kPa, for the second compression has increased from 0.06 to 0.065 and 0.08 for inter-fibre adhesion forces of 25 μN and $250\mu N$, respectively, compared to no increase in the network without fibre-fibre adhesion. We also see that the increased adhesion leads to a reduction in pressure for low SVF after which the curves quickly
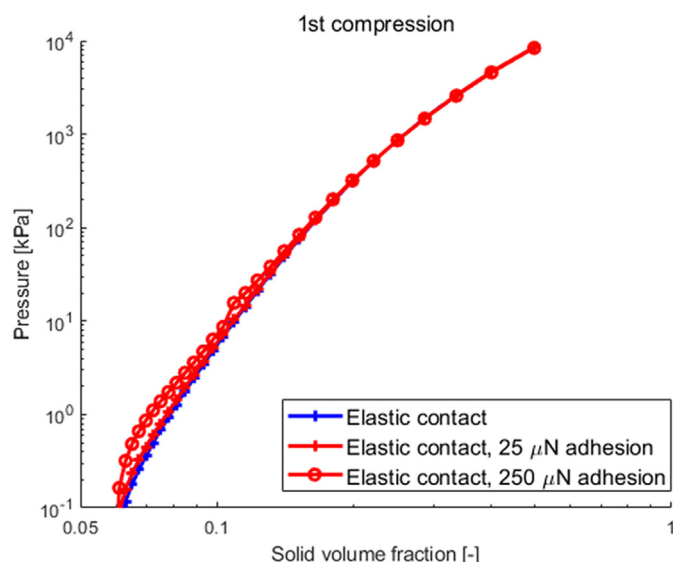
Fig. 7. The simulated first compression of networks with varying inter-fibre adhesion. In all the cases the fibres have elastic contacts. The results show a small impact on pressure development from increased adhesive force in the low SVF range after which the impact becomes negligible.

Fig. 9. Number of fibre-fibre contacts per fibre vs. solid volume fraction during unloading for two networks with inter-fibre adhesion compared to the case with elastic contacts. The number of contacts closely follows the elastic case during unloading before settling at a plateau at a level dependent on the magnitude of the adhesive force.
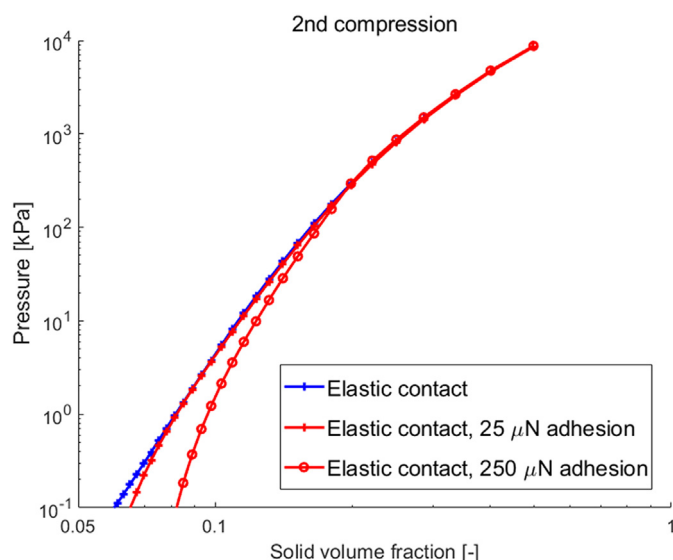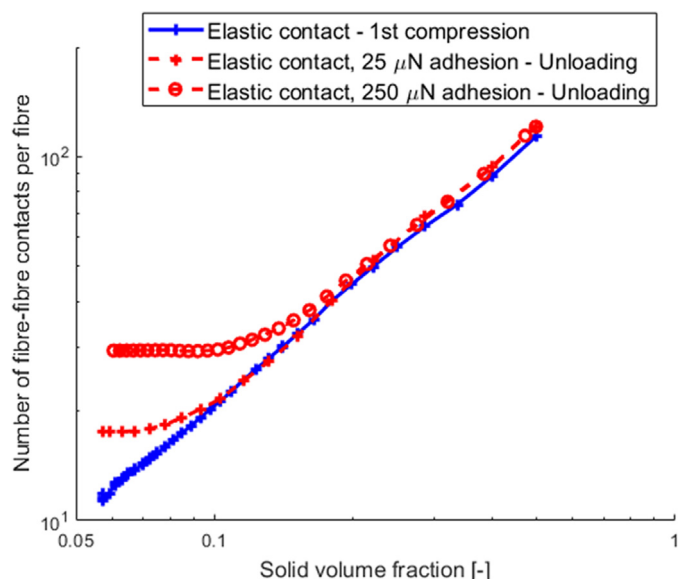

Fig. 8. The simulated second compression of networks with varying inter-fibre adhesion. In all the cases the fibres have elastic contacts. The increased magnitude of the adhesive force is seen to increase the degree of non-reversible deformation from the first compression in terms of initial solid volume fraction and decrease the pressures at low solid volume fractions.

closely follows the curve of the simulated case without adhesion. As the compressing wall is moved further, the SVF decreases and the curves for the cases with adhesion start to deviate from the case without adhesion leaving an increased number of fibre-fibre contacts remaining during unloading compared to the case without adhesion. As the compressing wall is moved even further away, the number of fibre-fibre contacts for the cases with adhesion settles at a plateau and the network loses contact with the compressing wall. The point at which the curve starts to deviate from the non-adhesive case, as well as the level of the plateau, are clearly dependent on the magnitude of the inter-fibre adhesive force, with networks settling at 18 and 29 fibre-fibre contacts per fibre for inter-fibre adhesion forces of 25 μN and 250μN, respectively, compared to the value of 12 contacts per fibre before compression. Note that SVF is here calculated as the ratio of the solid volume and the volume between the top and the bottom wall leading to the SVF value losing some of its meaning once the top wall loses contact with the network. The results show that the number of fibre-fibre contacts after compression and unloading does not return to the same value as before compression. This is a clear indication of non-reversible deformation of the network and that the degree of non-reversible deformation is dependent on the magnitude of the inter-fibre adhesive force. The deformation of the network after compression can also be represented visually as in [Fig. 10].

Next, we continue characterizing the effect of inter-fibre adhesion on non-reversible network deformation by studying a compression-unloading cycle up to a lower maximum compression. We use in this case a network with inter-fibre adhesion forces of 25 μN and compress it to a SVF of 0.12 in order to compare our simulations to the measurements from a lower degree of compression labelled "10 k Pa" in [Fig. 1]. The results show that after compression-unloading to a maximum SVF of 0.12 the number of remaining fibre-fibre contacts is on the same level as for the case with the same network being compressed to a SVF of 0.48, indicating that after a certain degree of compression no further non-reversible deformation is produced in the simulated network. Indications of this can also be seen in [Fig. 9] where the numbers of fibre-fibre contacts during unloading for the case with adhesion and the case without adhesion follow each other very closely from maximum compression down to a SVF of around 0.1. The rationale for the plateau in fibre-fibre contacts and the fact that in these simulations
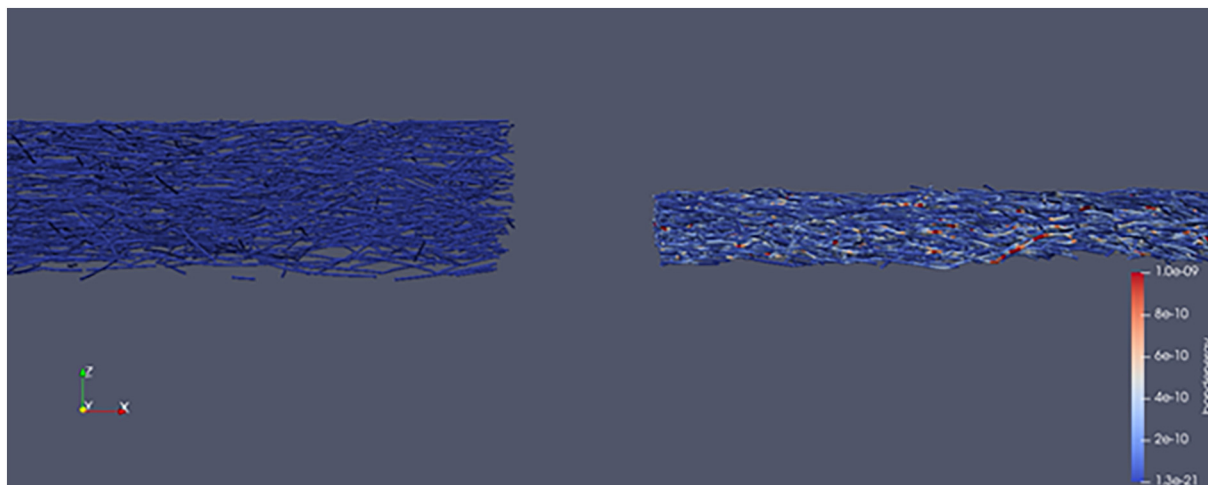
collapse as SVF is increased. These results indicate the existence of non-reversible deformation caused by the compression due to the presence of inter-fibre adhesion. However, we also note that the degree of non-reversible deformation of the simulated network is on a different level than what is seen in the measurements [Fig. 1] for both magnitudes of the adhesive force simulated. The source of the non-reversible deformation is further clarified when looking at a number of fibre-fibre contacts per fibre during unloading of the network [Fig. 9].

During compression, the number of fibre-fibre contacts follows the same curve as for the case with elastic contacts. If we follow the development of the number of fibre-fibre contacts during unloading (curves starting in the top right of [Fig. 9] going left) we see that, for the simulations with inter-fibre adhesion, that number initially decreases and

Fig. 10. Cross section view of slices from two networks after the cycle of compression-unloading. The left-hand network is from the case without inter-fibre adhesion and the right-hand network from a case with 250μN adhesion. Both networks are at equilibrium and not touching the upper wall (top and bottom wall removed for visibility). Fibres are coloured based on the fibre deformation energy (inter-fibre particle bond energy in normal, shear, twist and bend, see Eq. 6). The residual fibre deformation energy can be seen in the network with adhesion after unloading while in the network without adhesion fibres return to a relaxed state.

the compression beyond a certain SVF produces no further non-reversible deformation of the network lies in the breakage of fibre-fibre contacts during unloading. Non-reversible deformation after unloading is due to fibre-fibre contacts not breaking during unloading. The question of whether contacts break during unloading is determined by a competition between fibre deformation forces and moments acting to return the fibre to the original shape and fibre-fibre adhesion forces trying to keep the contact intact. At high SVF the fibre deformation forces and moments dominate over adhesion forces and, as a result, bonds break during unloading. However, as SVF is decreased, fibre deformation forces and moments decrease, and the network finally reaches a point where inter-fibre adhesion forces outweigh fibre deformation forces and moments. Then, inter-fibre contacts stop breaking and create a plateau in [Fig. 9] and consequently cause non-reversible deformation of the network. Evidence of this can also be seen in [Fig. 10] where fibres are coloured based on the fibre deformation energy after unloading. In the right-hand network with adhesion, the fibre deformation energy does not return to zero due to the adhesive contacts creating residual strain in the network after unloading. Such an effect can also be seen in [Fig. 11], where a network with one order of magnitude lower fibre stiffness has been simulated in the same way, resulting in a higher number of fibre-contacts retained after unloading for the same magnitude of inter-fibre adhesion.

To prove that the number of fibres used in the simulations is sufficient and that our results are not highly dependent on the areal density, we perform simulations with a varying number of fibres [Subset of Fig. 11]. Here we use the same reduced fibre stiffness as in [Fig. 11]. The networks consist of fibres with elastic contacts and 250 μN adhesion and contain 3000, 6000 and 12,000 fibres respectively. The results show a small influence of increasing the number of fibres. The increased areal density leads to a slight increase in non-reversible deformation as seen in the slight increase in the number of fibre-fibre contacts retained during unloading.

We conclude that for the simulated networks with elastic fibres, inter-fibre adhesion has a certain impact on non-reversible deformation. The degree of non-reversible deformation is dependent on the relationship between the adhesive force and fibre stiffness, with the higher magnitude of the former and lower fibre stiffness leading to an increase in non-reversible deformation after compression. The impact of adhesion is, however, limited to a low SVF range where the adhesive force can overcome the fibre deformation forces and moments. For compression beyond this point, no further non-reversible deformation is sustained. This indicates that inter-fibre adhesive forces help explain

non-reversible deformation for compression in the low SVF range, such as seen in the measurements labelled *10 kPa* in [Fig. 1]. The results also show that when using the adhesive force of 25 *μN*, no further
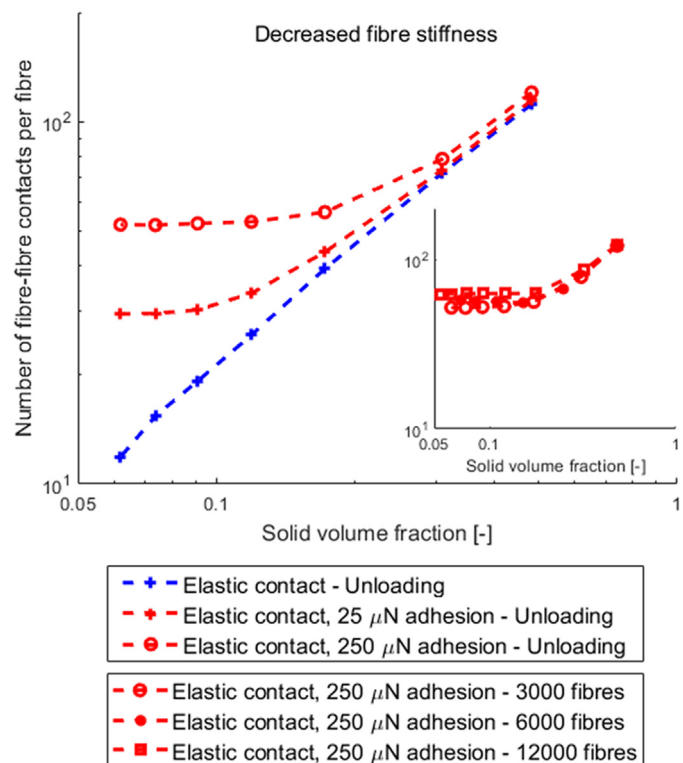

Fig. 11. Simulated network with fibre stiffness reduced by one order of magnitude. The number of fibre-fibre contacts per fibre vs. solid volume fraction is plotted during unloading for two networks with inter-fibre adhesion compared to the case with elastic contacts. The effect of reduction in fibre stiffness can be seen, leading to a higher number of fibre-fibre contacts remaining after unloading compared to the corresponding networks with stiffer fibres (see Fig. 9).

Subset of Fig. 11: Results showing number of fibre-fibre contacts per fibre during unloading for networks with varying areal density. The simulated networks with the same reduction in stiffness as above consisting of 3000, 6000 and 12,000 fibres in the 1x1cm area. The results show only marginal influence of areal density. Increasing the number of fibres leads to a slight increase in the number of fibre-fibre contacts retained after unloading.

non-reversible deformation is achieved for compression beyond SVF of around 0.1. Such a finding is not corresponding well with the measurements (see measurement labelled *1000 kPa* in [Fig. 1]), as it does not capture the deformation of the network due to compression to high SVF, again suggesting the impact of physics not accounted for in the simulations.

4.3. Network properties for elasto-plastic contacts

After concluding that the large non-reversible deformation seen in the measurements is not completely understood by assuming the fibres to have purely elastic contacts or elastic contacts with adhesion, we proceed to further investigate the origin of this deformation. The objective here is to characterize the role that elasto-plastic contacts play in the development of pressure and non-reversible deformation in a network from a first compression and to also see how pressure develops during a second loading. This is done by performing simulations of the same network while taking fibre contacts as elasto-plastic as described in Section 3.2. For the simulations we choose the criterion for plastic deformation by using the *yield ratio* values of 0.2 and 0.1.

Looking at the results for pressure vs. SVF [Fig. 12] for the first compression, we see that for networks with elasto-plastic deformation the pressure is unaffected in the low SVF-range, while at higher compression the pressure is reduced compared to the simulated network with elastic contacts, in line with the results previously reported by Guo et al. The effect is seen to be dependent on the yield criterion. A lower yield ratio (less fibre transverse compression required to yield) leads to a greater degree of reduction in the pressure. Also, the point at which the pressure for the elasto-plastic case starts to deviate from that in the elastic case is starting at a lower SVF. The results for the second compression with elasto-plastic deformation (the dashed line in [Fig. 12]) show that the pressure vs. SVF curve is reduced compared to the first compression in the entire SVF-range up to the point of the maximum pressure where the curves for the first and second compression coincide. The *initial solid volume fraction*, measured at 0.1 kPa, is increased to 0.09 compared to the original value of 0.06, indicating non-reversible deformation of the network. The rationale behind this reduction in the pressure during the second compression is the plastic
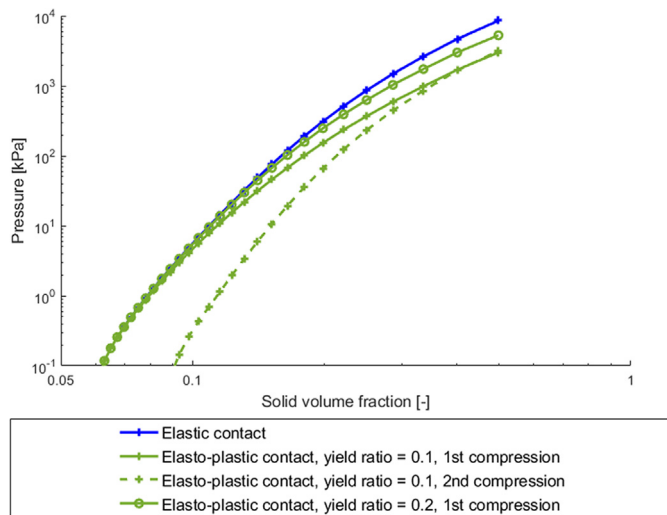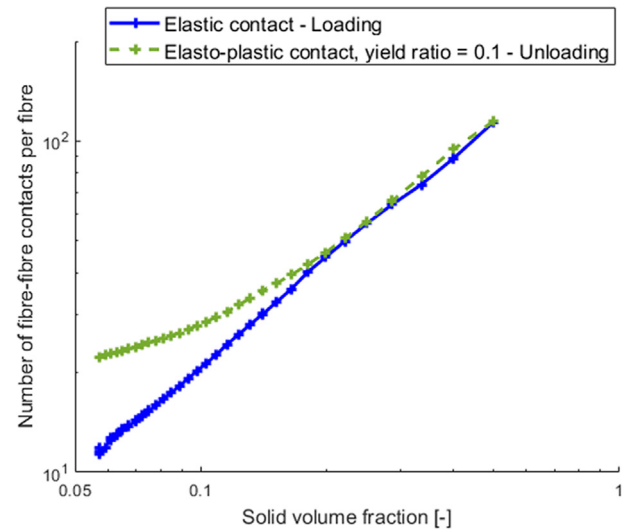

Fig. 13. Number of fibre-fibre contacts per fibre remaining during unloading of a network with elasto-plastic contacts compared to a network with elastic contacts. The results show signs of non-reversible deformation of the network due to the plastic deformation of fibres from the compression. We see an increase in the remaining fibre-fibre contacts after unloading which was not the case for the networks consisting of elastic fibres, see [Fig. 6].

deformation sustained by fibres from the first compression, which reduces the contact forces and effective radius of fibres at the points where plastic deformation has occurred. Since fibre networks with elasto-plastic contacts behave identically to networks with elastic contacts for cases where the yield criterion in the contact points is not exceeded, we note that no permanent deformation is sustained for compressions up to low SVF. For the simulated networks shown above, no significant non-reversible deformation is produced for compressions up to a maximum SVF of around 0.1 or less.

Looking at the number of fibre-fibre contacts of a network with elasto-plastic contacts, we see that during loading the number follows that of the case with elastic contacts. During unloading [Fig. 13:] the curve initially reverses following the path of the loading curve, while at lower SVF it deviates, leaving an increased number of fibre-fibre contacts. After unloading of the network, some 22 contacts per fibre remain, compared to 12 contacts per fibre before compression, showing signs of non-reversible deformation of the network due to the plastic deformation of fibres from the compression.

In conclusion, elasto-plastic contacts between fibres affect non-reversible deformation both in terms of pressure development and the *initial solid volume fraction* after compression of the network in the cases where the yield criterion in the contact points has been exceeded. The network pressure at high SVF is reduced compared to that in networks with elastic contacts. Also, for the second compression, the *initial solid volume fraction* is increased, and the network pressure is reduced compared to the first compression through the entire SVF range up to the maximum pressure. All these findings are in good agreement with the characteristics of measurements of compression up to high SVF (see measurements labelled *1000 kPa* in [Fig. 1]). However, as fibre networks with elasto-plastic contacts do not generate non-reversible deformation of the network for the cases where the yield criterion in the contact points is not exceeded, the elasto-plastic effect itself cannot replicate non-reversible deformation in the low-SVF range such as the one seen in, for example, measurements labelled *10 kPa* in [Fig. 1].

4.4. Network properties for elasto-plastic contacts with adhesion

After looking at networks with elastic contacts, elastic contacts with adhesion and elasto-plastic contacts between fibres, we have concluded that the impact of adhesion could explain non-reversible deformation

Fig. 12. Simulated compressions of networks with elasto-plastic contacts compared to a network with elastic contacts. The results for the first compression show that the pressure is unaffected in the low SVF-range. At higher compression, the pressure is reduced compared to the simulated network with elastic contacts. For the second compression, the pressure vs SVF curve is shown for a yield ratio of 0.1. The results show reduced pressure compared to the first compression in the entire SVF-range up to the point of the maximum pressure, where the curves for the first and second compression coincide.

for compression in the low-SVF range and that the impact of elasto-plastic contacts could be behind non-reversible deformation for compression in the high-SVF range. The next step we take is to look at the impact of networks with fibres having a combined effect of elasto-plastic contacts and inter-fibre adhesion. We therefore simulate a network consisting of fibres with a maximum adhesive force between fibres of 25 μN and a *yield ratio* of 0.1 for an easy comparison with the results from the previous two sections.

The results for the first compression of the network having elasto-plastic contacts with adhesion show close to no difference compared to the first compression of the network with elasto-plastic contacts without adhesion [Fig. 14]. The results mimic the comparison between elastic contacts and elastic contacts with 25 μN adhesion in [Fig. 7], again showing how adhesion has a very marginal impact on the first compression.

Looking at the results for the second compression of a network with elasto-plastic contacts with adhesion [Fig. 15], we see a notable impact on the pressure vs SVF curve compared to the first compression. The *initial solid volume fraction*, measured at 0.1 kPa, is increased from the original value of 0.06 to 0.15 showing significant non-reversible deformation and in essence reducing the network thickness to less than half the original thickness. For the simulated cases we note that, while adding inter-fibre adhesion to a network with elastic contacts gives only a marginal contribution to non-reversible deformation, adding the same effect to a network with elasto-plastic contacts results in a significant increase in non-reversible deformation sustained by the network and reduction in the development of the pressure for the second compression. To further clarify the source of the non-reversible deformation we study the development of fibre-fibre contacts during unloading [Fig. 16].

The results in [Fig. 16] show a very significant difference in fibre-fibre contacts retained after unloading for the case having the combined effects of elasto-plastic contacts with adhesion compared to the previously shown cases with only adhesive contacts or only elasto-plastic
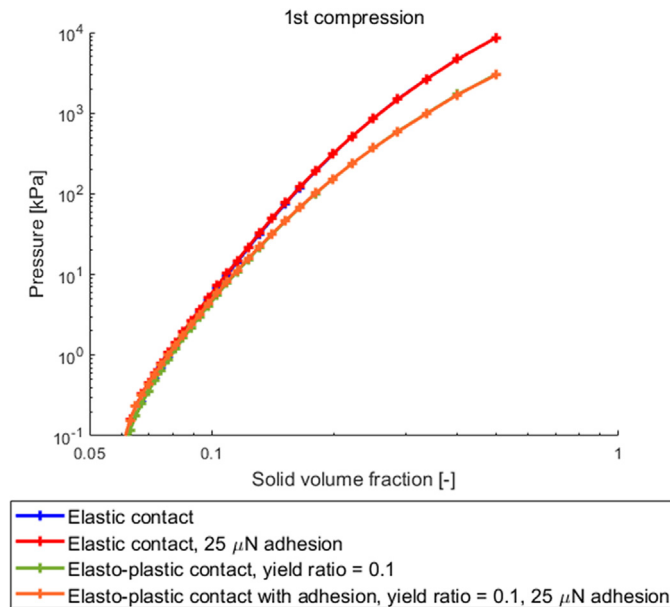

Fig. 15. Pressure development vs. solid volume fraction for the second compression of a network with elasto-plastic contacts with adhesion, compared to the three networks from previous results: Elastic contacts, elastic contacts with adhesion and elasto-plastic contacts. The results show a significant impact on non-reversible deformation in the network with elasto-plastic contacts with adhesion, both in terms of reduction in pressure and increase in the initial solid volume fraction.

contacts. The network having elasto-plastic contacts with adhesion retains 70 contacts per fibre after compression compared to the values of 18 and 22 for the networks with those two effects taken separately. The curve is similar to the previously shown cases with adhesion [Section 4.2] in that the number of contacts during unloading deviates from the loading curve and settles at a plateau. However, the added

Fig. 14. Pressure development vs. solid volume fraction for the first compression of a network with a combined effect of elasto-plastic contacts and adhesion compared to the three networks from previous results: Elastic contacts, elastic contacts with adhesion and elasto-plastic contacts. The results show that, for the first compression, adhesion with the chosen adhesive force has a marginal impact. The results for elasto-plastic contacts with adhesion overlap with the results from elasto-plastic contacts without adhesion in the same way as the results for elastic contacts with adhesion overlap with the results for elastic contacts without adhesion.
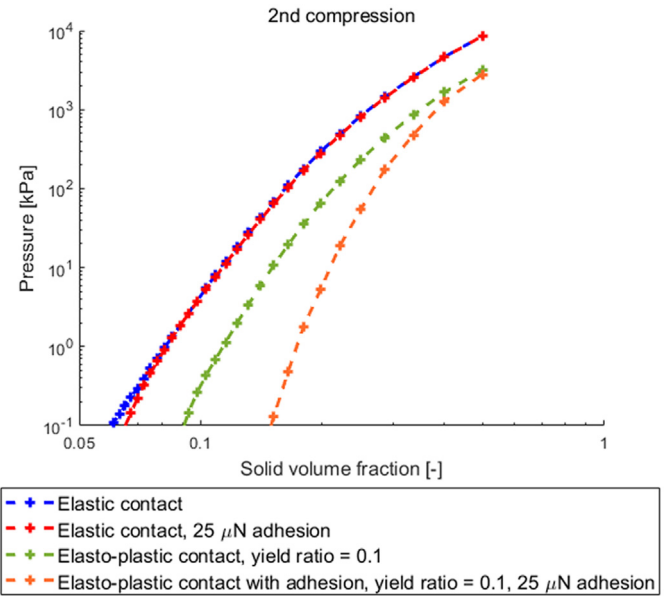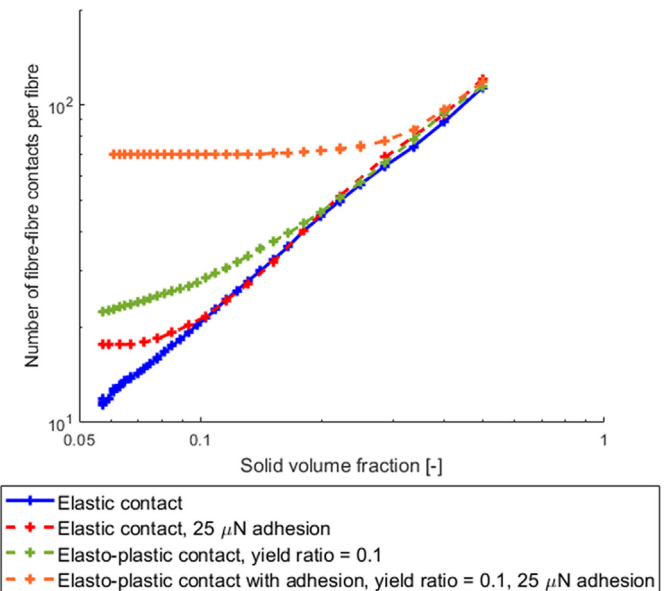

Fig. 16. Number of fibre-fibre contacts remaining during unloading of a network with elasto-plastic contacts with adhesion compared to the three networks from previous results: Elastic contacts, elastic contacts with adhesion and elasto-plastic contacts without adhesion. The contacts for the network having elasto-plastic contacts with adhesion settle at a plateau of 70 contacts per fibre indicating a significant impact on non-reversible deformation of the network.

effect of elasto-plastic contacts has clearly affected the breakage of adhesive contacts as the level of remaining contacts is increased.

To conclude, combining the effects of adhesion and elasto-plastic deformation of fibres clearly has an unambiguous synergetic effect. The results show an impact on non-reversible deformation seen both through a reduction of the pressure during a second compression and an increase in the *initial solid volume fraction* after first compression that is far beyond the sum of the individual contributions from including solely adhesion or elasto-plastic contacts. We argue that this synergetic impact stems from how the effects of adhesion and elasto-plastic contacts interact and reinforce each other.

Plastic deformation of contact points during loading of the network reduces the fibre-fibre contact pressure and the effective fibre diameter in these points permanently in the simulation. During unloading, the reduced contact pressure leads to adhesive contacts being retained to a greater degree as shown in [Fig. 16]. The reasoning behind this relates to the competition described in Section 4.2 between fibre deformation forces and moments acting to return the fibre to the original shape and fibre-fibre adhesion forces trying to keep the contact intact. The reduction in contact forces and the effective fibre radius essentially shifts the balance in that competition in favour of the adhesive forces, leading to an increase in the retained adhesive contacts. In this way, the effect of
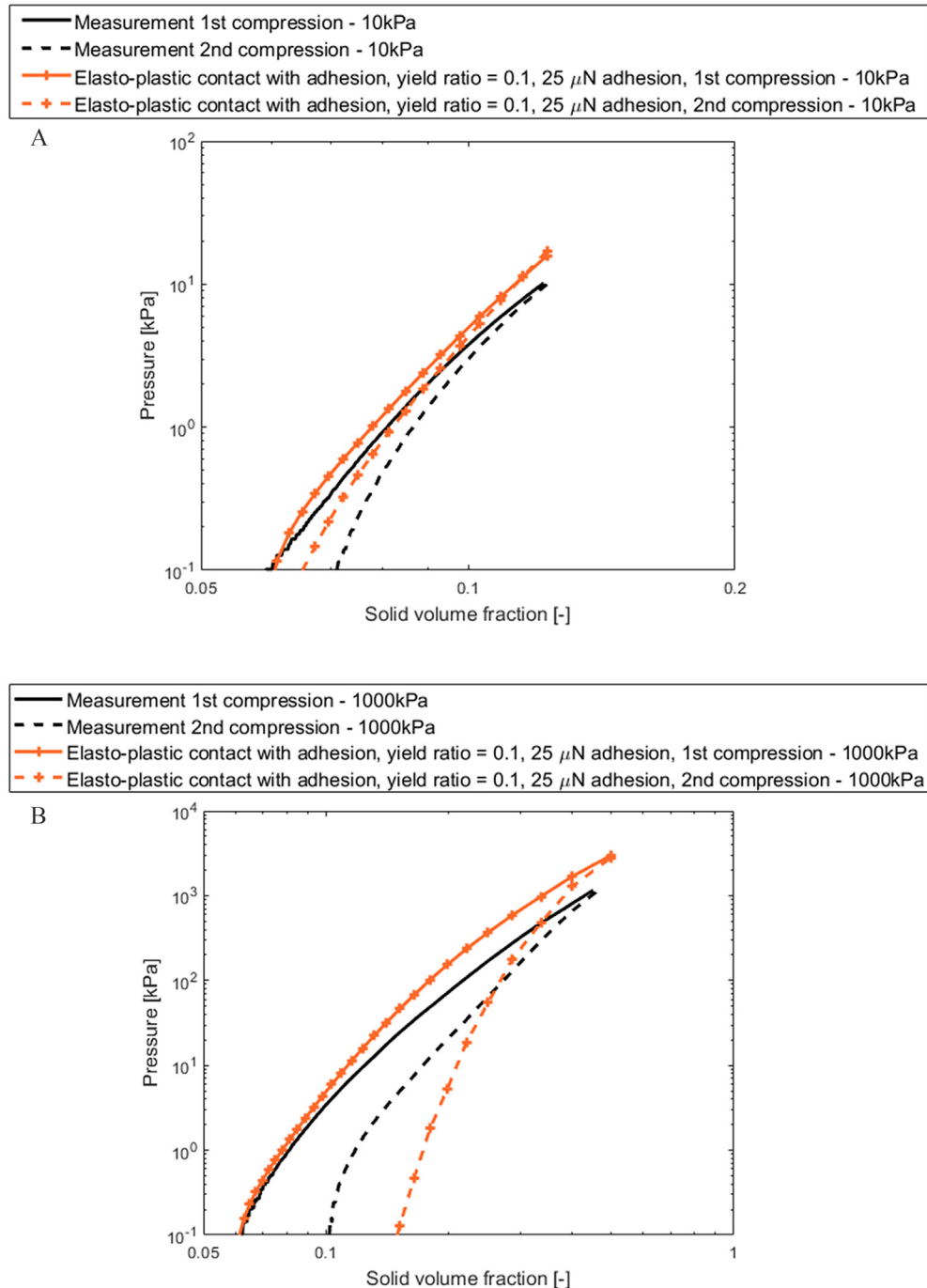

Fig. 17. Pressure development vs. solid volume fraction for measurements compared to simulations using the assumption of elasto-plastic contacts with adhesion. For clarity, the results are split into separate graphs (a): Comparison to measurements labelled "10 kPa". (b): Comparison to measurements labelled "1000 kPa".

inter-fibre adhesion is amplified by the plastic deformation in contact points.

At the same time, adhesive contacts remaining intact lead to less re-arrangement of fibres and contact points during unloading and during a second loading of the network. This effect ensures that the fibre-fibre contacts during a second loading happen in the exact same spot where plastic deformation of fibres has occurred during the first loading. This works to transfer the full effect of plastic deformation from a first loading to the pressure development of the second loading. The proof of this can be seen in [Fig. 15] looking at the pressure at the maximum compression for the network with elasto-plastic contacts compared to the network having elasto-plastic contacts with adhesion. The fact that the maximum pressures coincide for these cases for both first and second loading indicates that the addition of inter-fibre adhesion has not increased the degree of plastic deformation sustained in contact points as this would have reduced the pressure at a maximum compression. Instead, the impact of the plastic deformation has been amplified during the second loading leading to a reduction in pressure up to the final point where it coincides.

We summarize the main findings of this section in [Fig. 17]. We show that the combined effect of inter-fibre adhesion and elasto-plastic contacts correctly reproduces both compression to high solid volume fractions (SVF) and a lower degree of compression in terms of pressure development vs SVF and non-reversible deformation for first and second compressions of the network. We have shown that this is not the case for the cases where only elastic contacts, elastic contacts with adhesion or elasto-plastic contacts without adhesion were assumed.

5. Conclusions

We study in this paper non-reversible deformation due to large network strain from uniaxial compression in non-bonded, semi-flexible, anisotropic networks. We formulate a discrete element framework with bonded particles to characterize the impact of inter-fibre adhesion and elasto-plastic contacts. To validate our results, we performed measurements on a type of network often found in hygiene products consisting of air laid Southern Pine pulp fibres. The main conclusion that can be taken from our study is:

- We have found a clear synergetic effect of fibres having elasto-plastic contacts and adhesion where the included physical phenomena reinforce each other leading to a degree of non-reversible deformation of the network far beyond that of networks with only elasto-plastic fibre contacts or inter-fibre adhesion.

We have proven this synergetic effect through the following line of numerical experiments:

- If only elastic contacts between fibres are assumed, the simulated networks fail to exhibit non-reversible deformation due to compression. The *initial solid volume fraction* and pressure development during a second compression are largely unaffected compared to the first compression, in stark contrast to what is seen in the measurements.
- Adding inter-fibre adhesion has an effect on non-reversible deformation in the simulated networks. The impact of adhesion is, however, limited to a low solid volume fraction (SVF) range where the adhesive force can overcome the fibre deformation forces and moments. The point in SVF up to which adhesion impacts non-reversible deformation is determined by the relationship between the magnitude of the adhesive force and the fibre stiffness. For compression beyond this point, no further non-reversible deformation is sustained.
- If elasto-plastic nature of contacts between fibres is introduced into our framework without including adhesion, we observe an effect on non-reversible deformation in the cases with large network strain where the yield criterion in the contact points is exceeded. When yielding occurs, pressure development compared to the corresponding elastic case

is reduced for a first compression. Also, non-reversible deformation of the network is seen during a second compression both in terms of increased *initial solid volume fraction* and a reduction in pressure development compared to the first compression.

- Adding the combined effect of inter-fibre adhesion and elasto-plastic contact produces identical results to networks having elastic contacts with adhesion up to the point where the yield criterion is exceeded. Beyond this point, the non-reversible deformation sustained by the network is amplified compared to the individual cases of the networks having elastic fibres with adhesion or networks having elasto-plastic contacts without adhesion. The synergetic effect of adhesion and elastoplasticity that amplifies non-reversible deformation is explained by the following course of action:
  - o Plastic deformation decreases fibre-fibre contact forces.
  - o Decreased contact forces lead to adhesive contacts being retained to a greater degree during unloading of the network.
  - o Retained adhesive contacts lead to fibres rearranging less between the first and second loading.
  - o Less rearrangement of fibres and contact points lead to amplification of the effect of plastic deformation during a second loading.

- The simulations with the combined effect of inter-fibre adhesion and elasto-plastic contacts show the ability to replicate characteristics of measurements. This is seen for compression to high solid volume fractions (SVF), as well as lower degree of compression both in terms of pressure development vs SVF and non-reversible deformation for first and second compressions of the network.

Declaration of Competing Interest

The authors declare that they have no known competing financial interests or personal relationships that could have appeared to influence the work reported in this paper.

References

[1] R. Picu, Mechanics of random fiber networks—a review, Soft Matter 7 (15) (2011) 6768–6785.
[2] C. Van Wyk, 20—Note on the compressibility of wool, J. Text. Inst. Trans. 37 (12) (1946) T285–T292.
[3] T. Komori, K. Makishima, Numbers of fiber-to-fiber contacts in general fiber assemblies, Text. Res. J. 47 (1) (1977) 13–17.
[4] S. Toll, Packing mechanics of fiber reinforcements, Polym. Eng. Sci. 38 (8) (1998) 1337–1350.
[5] C. Barbier, R. Dendievel, D. Rodney, Role of friction in the mechanics of nonbonded fibrous materials, Phys. Rev. E 80 (1) (2009) 016115.
[6] E. Ban, et al., Softening in random networks of non-identical beams, J. Mech. Phys. Solids 87 (2016) 38–50.
[7] D. Rodney, M. Fivel, R. Dendievel, Discrete modeling of the mechanics of entangled materials, Phys. Rev. Lett. 95 (10) (2005) 108004.
[8] G. Subramanian, C.R. Picu, Mechanics of three-dimensional, nonbonded random fiber networks, Phys. Rev. E 83 (5) (2011) 056120.
[9] M.S. Hossain, P. Bergström, T. Uesaka, Uniaxial compression of three-dimensional entangled fibre networks: impacts of contact interactions, Model. Simul. Mater. Sci. Eng. 27 (1) (2018) 015006.
[10] Y. Guo, et al., An investigation on triaxial compression of flexible fiber packings, AICHE J. 66 (6) (2020) e16946.
[11] D. Head, A. Levine, F. MacKintosh, Distinct regimes of elastic response and deformation modes of cross-linked cytoskeletal and semiflexible polymer networks, Phys. Rev. E 68 (6) (2003) 061907.
[12] H.J. Chmielewski, O.A. Hamed, M. Haeussler, Plasticizing Formulation for Fluff Pulp and Plasticized Fluff Pulp Products Made Therefrom, 2010 Google Patents.
[13] M. Basler, et al., *Absorbent Paper Product Having Improved Embossing*. 2009 Google Patents.
[14] Y. Guo, et al., Discrete Element Method Model of Elastic Fiber Uniaxial Compression, arXiv preprint arXiv:1909.02927 2019.
[15] R. Picu, A. Sengab, Structural evolution and stability of non-crosslinked fiber networks with inter-fiber adhesion, Soft Matter 14 (12) (2018) 2254–2266.
[16] Y. Guo, et al., Discrete element simulation studies of angles of repose and shear flow of wet, flexible fibers, Soft Matter 14 (15) (2018) 2923–2937.
[17] V. Negi, R. Picu, Mechanical behavior of nonwoven non-crosslinked fibrous mats with adhesion and friction, Soft Matter 15 (29) (2019) 5951–5964.
[18] V. Negi, R. Picu, Mechanical behavior of cross-linked random fiber networks with inter-fiber adhesion, J. Mech. Phys. Solids 122 (2019) 418–434.

[19] Y. Guo, et al., A bonded sphero-cylinder model for the discrete element simulation of elasto-plastic fibers, Chem. Eng. Sci. 175 (2018) 118–129.

[20] T. Leblicq, et al., A discrete element approach for modelling the compression of crop stems, Comput. Electron. Agric. 123 (2016) 80–88.

[21] Y. Guo, et al., Discrete element method models of elastic and elasto-plastic fiber assemblies, AICHE J. (2021) e17296.

[22] J. Lindau, H. Theliander, K. Sjöström, The compression of pulp before and during brown stock washing–its influence on fibre properties, Nord. Pulp Pap. Res. J. 23 (2) (2008) 195–201.

[23] EDANA, EDANA Standard Procedure NWSP 120.6.R0, Available from https://www.edana.org/docs/default-source/international-standards/table-of-content-nw-standard-procedures-20210105.pdf?sfvrsn=4ede1add_20 2015.

[24] C. Kloss, et al., Models, algorithms and validation for opensource DEM and CFD–DEM, Prog. Comput. Fluid Dyn. Int. J. 12 (2–3) (2012) 140–152.

[25] C. Richter, Liggghts-with-Bonds. GitHub Repository, https://github.com/richti83/LIGGGHTS-WITH-BONDS 2015.

[26] M. Schramm, et al., Estimating bond damping and bond Young's modulus for a flexible wheat straw discrete element method model, Biosyst. Eng. 186 (2019) 349–355.

[27] B.N. Persson, et al., Adhesion of cellulose fibers in paper, J. Phys. Condens. Matter 25 (4) (2012) 045002.

[28] C. Thornton, Z. Ning, A theoretical model for the stick/bounce behaviour of adhesive, elastic-plastic spheres, Powder Technol. 99 (2) (1998) 154–162.

[29] J.C. Loh, W.R. Ketterhagen, J.A. Elliott, A hybrid tabulation-scaling implementation of Thornton and Ning's plastic–adhesive particle contact theory, Powder Technol. 264 (2014) 599–607.

[30] T. Mikami, H. Kamiya, M. Horio, Numerical simulation of cohesive powder behavior in a fluidized bed, Chem. Eng. Sci. 53 (10) (1998) 1927–1940.

[31] S.R. Andersson, Network Disruption and Turbulence in Fibre Suspensions, Chalmers University of Technology, 1998.

[32] Y.I. Rabinovich, M.S. Esayanur, B.M. Moudgil, Capillary forces between two spheres with a fixed volume liquid bridge: theory and experiment, Langmuir 21 (24) (2005) 10992–10997.

[33] K. Washino, et al., A new contact liquid dispersion model for discrete particle simulation, Chem. Eng. Res. Des. 110 (2016) 123–130.

[34] R. Picu, G. Subramanian, Correlated heterogeneous deformation of entangled fiber networks, Phys. Rev. E 84 (3) (2011) 031904.

[35] C. Lorbach, et al., Pulp fiber bending stiffness in wet and dry state measured from moment of inertia and modulus of elasticity, BioResources 9 (3) (2014) 5511–5528.

[36] A. Abd El-Rahman, C. Tucker III, Mechanics of random discontinuous long-fiber thermoplastics. Part II: direct simulation of uniaxial compression, J. Rheol. 57 (5) (2013) 1463–1489.